Construction and Building Materials 136 (2017) 286–297

Contents lists available at ScienceDirect

Construction and Building Materials

journal homepage: www.elsevier.com/locate/conbuildmat

Improving the rheometry of rubberized bitumen: experimental and computation fluid dynamics studies

D. Lo Presti *, G. Giancontieri, D.M. Hargreaves

Faculty of Engineering, University of Nottingham, Nottingham NG7 2RD, UK

HIGHLIGHTS

- Background on viscosity measurements and CFD studies on mixing complex fluids.
- Laboratory tests provide visual proves of enhanced mixing efficiency with DHI.
- CFD models validated the empirical calibration with single phase fluids.
- CFD simulations compared well with experimental results.
- CFD clarifies reasons behind the improved rheometry of complex fluids with DHI.

ARTICLE INFO

Article history:
Received 17 May 2016
Received in revised form 1 December 2016
Accepted 29 December 2016

Keywords:
Asphalt rubber
Rubberized bitumen
CFD
Rheometry
Complex fluids
Viscosity

ABSTRACT

Multi-phase materials are common in several fields of engineering and rheological measurements are intensively adopted for their development and quality control. Unfortunately, due to the complexity of these materials, accurate measurements can be challenging. This is the case of bitumen-rubber blends used in civil engineering as binders for several applications such as asphalt concrete for road pavements but recently also for roofing membranes. These materials can be considered as heterogeneous blends of fluid and particles with different densities. Due to this nature the two components tends to separate and this phenomenon can be enhanced with inappropriate design and mixing. This is the reason behind the need of efficient dispersion and distribution during their manufacturing and it also explains while real-time viscosity measurements could provide misleading results. To overcome this problem, in a previous research effort, a Dual Helical Impeller (DHI) for a Brookfield viscometer was specifically designed, calibrated and manufactured. The DHI showed to provide a more stable trend of measurements and these were identified as being "more realistic" when compared with those obtained with standard concentric cylinder testing geometries, over a wide range of viscosities. However, a fundamental understanding of the reasons behind this improvement is lacking and this paper aims at filling these gaps. Hence, in this study a tailored experimental programme resembling the bitumen-rubber system together with a bespoke Computational Fluid Dynamics (CFD) model are used to provide insights into DHI applicability to perform viscosity measurements with multi-phase fluids as well as to validate its empirical calibration procedure. A qualitative comparison between the laboratory results and CFD simulations proved encouraging and this was enhanced with quantitative estimations of the mixing efficiency of both systems. The results proved that CFD model is capable of simulating these systems and the obtained simulations gave insights into the flow fields created by the DHI. It is now clear that DHI uses its inner screw to create a vertical dragging of particles within a fluid of lower density, while the outer screw transports the suspended particles down. This induced flow helps keeping the test sample less heterogeneous and this in turns allows recording more stable viscosity measurements.

This work was supported by the Engineering and Physical Sciences Research Council (EPSRC) [grant number EP/M506588/1].

1. Introduction

Rheological properties and their measurement are of paramount importance for the development, performance and applications of products across a wide range of industries. More

* Corresponding author.
E-mail addresses: davide.lopresti@nottingham.ac.uk (D. Lo Presti), Gaspare.Giancontieri@nottingham.ac.uk (G. Giancontieri), david.hargreaves@nottingham.ac.uk (D.M. Hargreaves).

http://dx.doi.org/10.1016/j.conbuildmat.2016.12.200
0950-0618/

specifically, bitumen technologists are used to monitoring the high-temperature viscosity of these binders (in the range 100–200 °C) during manufacture, compaction and quality control [6]. Furthermore, the use of bituminous binders modified with polymers is a common practice used to enhance the performance of road pavements and roofing membranes. Nevertheless, measurements of their viscosity/rheology can be challenging due to the often heterogeneous structure of these complex systems, especially if these materials suffer from phase stratification within the time frame of typical viscosity measurements, as in the case of rubberized bitumen [7].

A common instrument used to perform these measurements is the rotational viscometer, typically by means of the coaxial cylinder testing geometry. This setup consists of a static outer cylindrical vessel into which is poured the test fluid and a concentric cylinder (spindle) which is inserted and then rotated at a given angular velocity so that the applied torque can be measured. A standard cylindrical spindle that can be used in the Brookfield viscometer is shown in Fig. 1(a). This arrangement, however, is incapable of providing reliable viscosity measurements of multiphase systems containing suspended particles with a density different to that of the continuous phase [19]. In fact, when standard cylindrical spindles are used to measure viscosity of fluids with suspended solid particles, if the two phases have very different densities the higher density component will tend to settle to the bottom during the measurement rendering the data acquired of very little use.

These type of scenarios are encountered in many type of complex systems such as: chocolate, plastic, rubber, ceramics, food, cosmetics, detergents, paints, glazings, lubricants, inks, adhesives and sealants [12,13,17,20,27]. Rotational viscometers (Brookfield in this case) are provided with supplementary spindle designs that help in some of these cases. For instance, a vane spindle allows performing measurements with paste-like materials, gels, and fluids where suspended solids migrate away from the measurement surface of standard spindles. Furthermore, the Brookfield Helipath Stand is designed to slowly lower or raise a Brookfield T-bar spindle so that it describes a helical path through the test sample. Nevertheless, these accessories are not designed to minimize the heterogeneity of multiphase blends, especially when that sample has the tendency to stratify due to phase density differences.

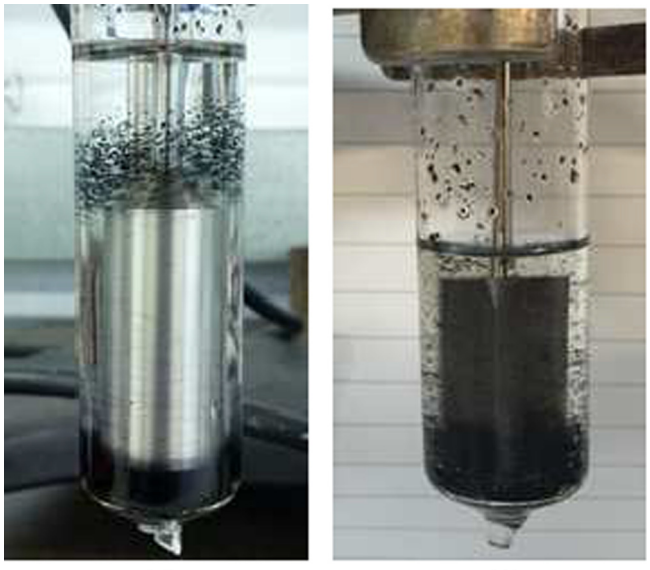

Fig. 1. Visualisation of the phase separation during viscosity measurements of suspensions for (a) the SC4-27 spindle and (b) a vane spindle.

Fig. 1(b) shows the inefficiency of the vane spindle when used for viscosity measurements of suspensions. In an effort to improve the rheometry of these scenarios by overcoming sample's phase separation issues, Lo Presti et al. [19] successfully designed, manufactured and tested a prototype of a Dual Helical Impeller (DHI) for Brookfield Rotational Viscometers (Fig. 2, right). Experimental studies were carried out to evaluate whether the DHI is able to improve the degree of homogenisation of high viscous fluids in order to obtain more realistic viscosity measurements of a blend of fluid with suspended particles. In comparison to the Brookfield standard, cylindrical geometry (spindle SC4-27), the DHI always predicted a different "apparent" viscosity (see Section 1.1 for definition). This result was explained by the capability of the DHI to create what have been likened to convective flows as opposed to the axisymmetric swirling flow induced by the standard SC4-27 spindle.

Rubberised bitumen is a complex system of the type described above, where the bitumen is the fluid matrix and the particles are the swollen tyre rubber crumbs. These two components have a moderate difference in densities and for this reason the phase separation could not possibly occur within standard rotational viscosity measurements at 135 °C. However if long equilibrium times are required, rather than high percentage of modifier, higher testing temperatures and high spindle speeds, the phase separation issue is very likely to occur, especially for a wet process-high viscosity binder. Furthermore, this issue is particularly relevant within the product development of rubberised binder with rotational viscometer used as a mixing device offering a continuous monitoring of the viscosity [7,26]. In fact, in this scenario the processing is made at high rotational speed and at a temperature where the bitumen viscosity is quite low (180 °C) and rubber particles are not swollen yet and tend to agglomerate in layers, mainly at the bottom of the tube. The DHI presented above was developed [19] specifically to solve this type of issue within low-shear development of rubberised bitumen. This research showed that carrying out measurements of rubberised bitumen with the DHI at 135 °C reduces the initial effort needed to accelerate a bitumen-rubber blend from a stationary position and provide more stable viscosity readings. This allowed the authors to declare that this type of measurements were "more realistic" (Fig. 3). However, despite these satisfying results, the mechanisms behind the enhanced mixing efficiency provided by the DHI and the actual level of enhancement were not clear and this present study aims to clarify.

In order to provide the reader with further information for the interpretation of the presented results and conclusions, the following sections will provide a background on measuring viscosity by means of a rotational viscometer and a brief review on the use of CFD for modelling mixing of complex fluids.

1.1. Background – Measuring viscosity by means of a rotational viscometer

For the rheological measurement of materials by means of a rotational viscometer with a coaxial cylindrical geometry, there is a theoretical basis for the calculation of the viscosity. Consider a cylinder of radius R_s and length, L_s, rotating at an angular velocity, ω, inside a stationary cylinder of radius, R_c. The shear rate at the surface of the spindle, $\dot{\gamma}$, is

$$\dot{\gamma} = \frac{2\omega R_c^2}{R_c^2 - R_s^2}, \tag{1}$$

and the shear stress, τ, is

$$\tau = \frac{T}{2\pi R_s^2 L}, \tag{2}$$

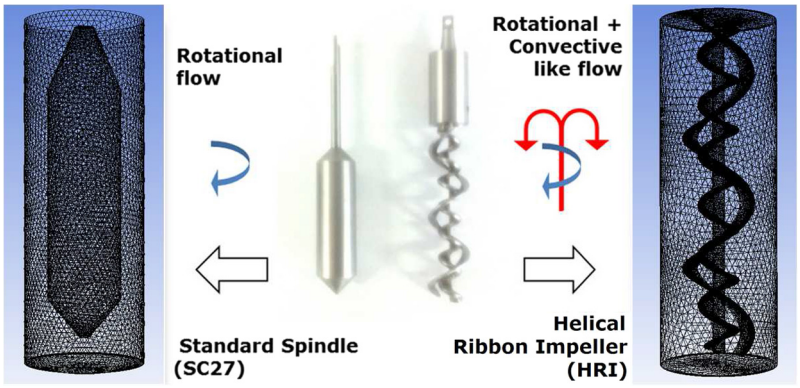

Fig. 2. On the left, the standard SC27 spindle and associated surface mesh; on the right, the Dual Helical Ribbon Impellor (DHRI) and mesh.

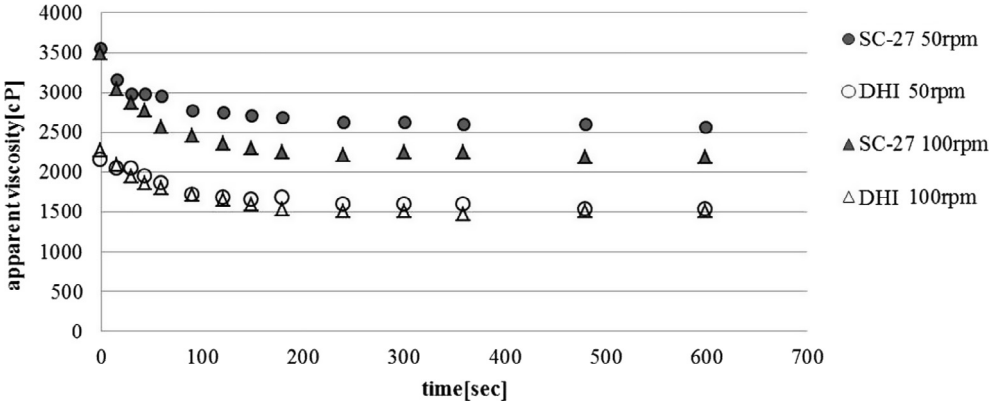

Fig. 3. Apparent viscosity of a TR-MB at 180 °C using a rotational viscometer at 50 to 100 rpm [19].

where T is the torque input by the machine. The viscosity, μ, is

$$\mu = \frac{\tau}{\dot{\gamma}} = \frac{T(R_c^2 - R_s^2)}{4\pi\omega R_c^2 R_s^2 L}. \tag{3}$$

So, since all the variables on the right-hand-side of Eq. (3) are measurable, the viscosity can easily and reliably be determined.

Now, when an non-cylindrical impeller is used in the viscometer, there are no tractable equations for the shear rate or shear stress akin to Eqs. (1) and (2). This presents a challenge since, while the impellers may be good at mixing, there is no simple way of analytically determining the viscosity of the mixture. The only quantities that can be measured directly are the torque, T, and the angular velocity, ω.

In this case, one way to proceed is to calibrate the impeller using a range of single and multi-phase fluids of known viscosity, which may have been measured with the standard spindle viscometer. Then, the viscosity becomes a function of the two measurable variables

$$\mu = \mu(T, \omega). \tag{4}$$

There is no information about the shear rate or the shear stress that can be derived because the complex 3D nature of the flow precludes that. After testing a wide range of fluids of different viscosities, a surface fit could be made and then for a given T and ω, the viscosity of an unknown fluid could be calculated. The situation is further complicated in that the calibration procedure would then have to be done for each class of fluid (Newtonian, shear thinning, shear thickening, etc.) and a judgement would have to be made by the user as to which class of fluid they had in the viscometer.

A different approach is that promoted by Brookfield and utilized, for example, in Lo Presti et al. [19]. Each different spindle geometry provided by Brookfield for use in their viscometers is ascribed a Spindle Multiplier Constant (SMC) value. For example, the SC4-27 has an SMC of 25. Further, each viscometer model, here we are using the LVDV-E, has a Torque Constant, TK, which allows the apparent viscosity to be found from

$$\mu = \frac{0.1}{N} \cdot \mathrm{TK} \cdot \mathrm{SMC} \cdot \mathrm{T\%}, \tag{5}$$

where N is the rotational speed (rpm) and T% is percentage of the maximum spring torque that the viscometer can deliver. In addition, the Strain Rate Constant (SRC) is defined as

$$\dot{\gamma} = \mathrm{SRC} \cdot N = \mathrm{SRC} \cdot \left(\frac{60}{2\pi}\right)\omega. \tag{6}$$

Equating (1) and (6) allows us to write

$$\mathrm{SRC} = \frac{\pi}{15}\frac{R_c^2}{R_c^2 - R_s^2}, \tag{7}$$

which, when the dimensions of the SC4-27 spindle and its container (Fig. 4) are considered, results in a value of 0.34, which tallies with that in Brookfield's literature [5].

For a design such as a DHI, this is a simplification but one which can produce values of apparent viscosity that are of practical use. Lo Presti et al. [19] attempted, with some success, to match the behaviour of the DHI to the range of SC-XX spindles offered by Brookfield. The SC4-XX range are of the cylindrical type and each has unique SRC and SMC values. The Brookfield viscometer allows only the selection of a spindle code, which has associated SRC and

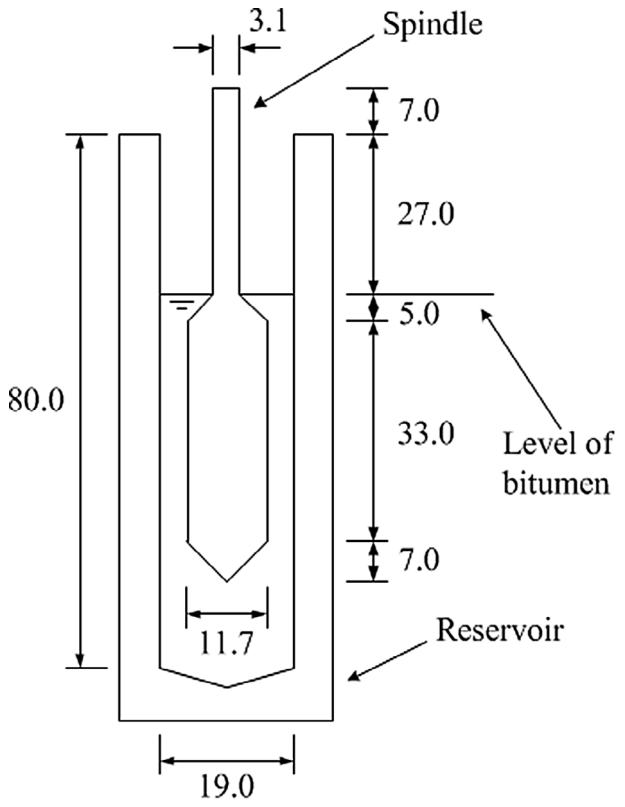

Fig. 4. A schematic of the Brookfield SC4-27 spindle.

SMC values, thus limiting fine adjustment to a discrete set of values. Lo Presti et al. [19] were nevertheless able to find a spindle code that matched closely the DHI and did this by testing the DHI against a number of standard liquids of known viscosity. The SC4-28 spindle was found to most closely match the DHI with values of SRC of 0.28 and SMC of 50. The validity of this approach is open to question because of the radically differing spindle geometries of the SC4-28 and DHI. Thus, computational fluid dynamics was seen as an alternative method of obtaining values of SRC and SMC for the DHI geometry.

1.2. Background – CFD modelling of the mixing of complex fluids

The mixing of two or more miscible phases, whether it be solid/liquid, gas/liquid or liquid/gas or combinations thereof, are widely encountered in mineral, food, pharmaceutical, polymer, metallurgical, biochemical, and other industrial processes [23]. The mixing of highly viscous fluids is often carried out in the laminar and transition regimes. Many impellers were proposed by researchers based either on using large impeller diameters or close-clearance designs like anchors and helical ribbons [9,14,8,30,24].

Generally, this mixing is carried out in stirred vessels and it has been reported that the so-called helical ribbon and helical screw impellers are most appropriate for efficient mixing of high viscosity Newtonian [22] and non-Newtonian liquids [33]. Before the development of numerical simulations, mixers were normally evaluated experimentally using various measures: power consumption (e.g. [29,27]); mixing time (e.g. [28,26]); and circulation time.

However, none of these measures give an understanding of the spatial variation of the phases or the nature of the transport processes, making the understanding and hence the efficient optimisation of the mixer design difficult. Numerical simulations offer a greater flexibility in analysing and visualising the mixing. In recent years, the simulation of mixing vessels is widely used to optimize mixer geometries and get better insights of the complex flow patterns generated by the impeller-vessel wall interaction [30,24]. From the perspective of numerical analysis, one of the pioneering CFD works focused on the mixing performance of helical ribbon impellers in cylindrical vessels is the contribution made by Tanguy et al. [29]. They developed a three-dimensional model, which was validated experimentally, based on the finite-element method for the analysis of a Helical Ribbon-screw impeller. The authors reported good liquid circulation at low impeller speeds (10 rpm) and showed evidence of poor pumping in the vessel bottom. They noticed that the segregation increased upon increasing the impeller speed. In subsequent work numerical models were developed for several helical ribbon geometries and fluids of rheological behaviours [4]. The numerical modelling of mixing in a stirred tank has attracted a great deal of attention and a review of the state-of- the-art in CFD simulations of stirred vessels can be found in Sommerfeld and Decker [25].

The rapid development of numerical techniques and computational power has unleashed the possibilities of Computational Fluid Dynamics (CFD) in this area. CFD is now an important tool for understanding the mixing in stirred tanks [31]. Nevertheless, modelling of the complex flow in the presence of a rotating impeller is a computational challenge because of the complex geometry of the impeller and the nature of the flow in stirred tanks. Although CFD codes have made remarkable steps towards the solution of such engineering problems over the last decade, it still remains a difficult task to use such codes to help the design and the analysis of stirred tanks. Iranshahi et al. [16] investigated the flow patterns and mixing progress in a vessel equipped with a Maxblend impeller in the case of Newtonian fluids. In that study, they found that the Maxblend impeller showed good performance when used with baffles in the transition and laminar regimes. In another study, a CFD characterization of the hydrodynamics of the Maxblend impeller with Newtonian and non-Newtonian inelastic fluids in the laminar and transition regimes was carried out by Devals et al. [11]. In that study, the effect of the impeller bottom clearance and the Reynolds number on the power characteristics, the distribution of shear rates and the overall flow condition in the vessel were investigated. Yao et al. [32] performed numerical analysis for the local and total dispersive mixing performance in a stirring tank with a standard type of Maxblend and double helical ribbon impellers. They showed that the double Helical Ribbon cannot be an efficient dispersive mixer – however, the results were not validated by experimental tests.

Iranshahi et al. [15] investigated the fluid flow in a vessel stirred with a Ekato Paravisc impeller in the laminar regime using CFD. The viscous mixing characteristics of the Ekato Paravisc were compared with those of an anchor and a double helical ribbon. They were able to show, through a number of experimentally validated criteria, that the Paravisc impeller was capable of producing homogeneous mixtures. Numerical modelling was carried out by Bertrand et al. [4] to predict a rise in power draw due to elasticity. They explained the numerical methodology and compared the results of the simulation with experimental tests in the case of a stirred tank with a helical ribbon. Barailler et al. [3] performed CFD modelling of a rotor–stator mixer in the laminar regime. In this study they investigated the characteristics of the rotor–stator mixing head in the case of viscous Newtonian fluids. Delaplace et al. [10] developed an approximate analytical model based on the Couette flow analogy to predict power consumption for the mixing of pseudoplastic fluids with helical ribbon and helical screw ribbon impellers in the laminar regime. They presented extensive comparisons between the predicted results and the data which was reported in the existing literature.

1.3. Aims and structure of the paper

This paper presents a Computational Fluid Dynamics (CFD) model able to reproduce the observations obtained from a laboratory investigation aimed at resembling a bitumen-rubber system during product development over a wide range of testing conditions (e.g. temperatures, particle contents, impeller speed). In order to allow visual inspections, the experimental programme was performed by using tyre rubber particles and transparent fluids having viscosities similar to the bitumen phase of rubberised binder at manufacturing and testing temperatures. The overall objective of the present study is to assess whether a CFD model would be able to simulate this complex scenario and to couple these outcomes with visual images to shed light on the results obtained in a previous study [19], where the DHI provided "more realistic" viscosity measurements when compared to the standard spindle. By doing this, we aim to highlight the benefits and limitations of using the DHI geometry to perform viscosity measurements of complex fluids, as well as using the model to validating the empirical calibration procedure (SMC and SRC).

Section 2 introduces a brief description of the experiments along with the numerical framework and governing equations for the CFD model. The results of the experimental and numerical modelling, along with a discussion thereof, are presented in Section 3, which ultimately aims to validate the numerical model. Finally, conclusions are presented in Section 4 with some thoughts about the next steps in this programme of work.

2. Methodology

2.1. Experimental campaign

As mentioned earlier, in a previous investigation experimental studies were carried out to calibrate the DHI and to evaluate the improved mixing when used in a Brookfield viscometer [19]. In order to allow visualisation of the movement of particles in the system, the viscometer was customised with a transparent outer cyclinder (e.g. Fig. 1). The experimental programme used multiphase fluids made up of a range of standard viscosity fluids and tyre rubber particles.

Thus, nine different complex fluids were made from the combination of different standard-viscosity fluids and different diameter tyre rubber particles (Table. 1)– all fluids being tested at 10, 100 and 200 rpm at ambient temperature (20 °C). The range of viscosity and particle diameters have been chosen in order to recreate systems similar in terms of viscosity and physical composition to tyre rubber-bitumen blends at temperatures between 100 and 200 °C. This is considered to be representative of the possible scenarios occurring during the low shear modification of bitumen with crumb rubber particles [18].

Due to the expected high torque, which would be close to the viscometer's limits, the tests with the f500 fluid were performed up to 100 rpm. Tests were conducted according to Subhy et al. [26], which are based on international standards on viscosity measurements of a rubberized bitumen (asphalt rubber) [1,2]. These were undertaken for durations of between 15 and 20 minutes, depending on how quickly the mixing was seen to reach a steady distribution. The particles were added to the fluid and the blend was shaken to produce an even distribution of the particles. In these conditions, the impellers were quickly submerged in the blend and the viscometer was turned on to carry out the test, during which torque and angular velocity were measured and the viscosity calculated from Eq. (3).

Results were compared against those obtained with a standard spindle, SC4-27, to establish which geometry produced the highest degree of homogenisation and hence the more realistic, repeatable and reliable viscosity measurements.

Table 1
Fluid and particle properties.

Name	Fluid		Particles	
	Density (kg m^{-3})	Viscosity (Pa s)	Diameter (μm)	Volume fraction
f10	940	0.01	200	1%
f100	960	0.1	400	3%
f500	970	0.5	1000	5%

2.2. CFD simulations

In parallel with these experiments, a CFD study was conducted with the aim of qualitatively comparing the two sets of results. Version 14 of ANSYS Fluent, the commercially available CFD software, was used in this work.

2.2.1. Governing equations

The modelling involves the solution of the Navier–Stokes equations, which are based on the assumptions of conservation of mass and momentum within a moving fluid. In order to simulate the behaviour of the complex, two phase fluids in the present application, the mixture model was used. Here, the momentum and continuity equations are solved for the mixture, the volume fraction equations for the secondary phases, while algebraic expressions are used for the relative velocities and inter-phase drag. The mixture model lends itself to particle-laden flows with relatively low volume loading, which is the situation in the present work.

First the mixture continuity equation

$$\frac{\partial \rho_m}{\partial t} + \nabla \cdot (\rho_m \mathbf{u}) = 0, \tag{8}$$

where $\mathbf{u}$ is the velocity, ρ is the density and the subscript m indicates a quantity defined for the mixture. The mixture velocity is a mass-weighted average of the n phases

$$\mathbf{u}_m = \frac{1}{\rho_m} \sum_{k=1}^{n} \alpha_k \rho_k \mathbf{u}_k, \tag{9}$$

where α is the volume fraction and k refers to the kth phase. The mixture density is

$$\rho_m = \sum_{k=1}^{n} \alpha_k \rho_k. \tag{10}$$

The momentum equation is

$$\frac{\partial}{\partial t}(\rho_m \mathbf{u}_m) + \nabla \cdot (\rho_m \mathbf{u}_m \mathbf{u}_m) = \nabla p + \nabla \cdot \left[\mu_m (\nabla \mathbf{u}_m + \nabla \mathbf{u}_m^T)\right] + \rho_m \mathbf{g} + \nabla \cdot \left(\sum_{k=2}^{n} \alpha_k \rho_k \mathbf{u}_{\mathrm{dr},k} \mathbf{u}_{\mathrm{dr},k} \right), \tag{11}$$

where $\mathbf{g}$ is the gravitational acceleration and $\mathbf{u}_{\mathrm{dr},k}$ is the drift velocity for the secondary phase k,

$$\mathbf{u}_{\mathrm{dr},k} = \mathbf{u}_k - \mathbf{u}_m. \tag{12}$$

The mixture model in ANSYS FLUENT uses an algebraic slip formulation, which is based on the work of Manninen et al. [21]. It uses the slip velocity, which is related on the drift velocity defined in Eq. (12). The velocity of the kth phase is calculated from algebraic expressions, rather than a separate momentum equation. So, the final term on the right hand side of Eq. (11) imparts a momentum source or sink to the mixture momemtum equation,

based on the relative motion of the primary and secondary phases. In the present work, the viscosity of the two phases are assumed to be equal to that of the primary, bituminous phase.

2.3. CFD model setup

It is accepted practice in stirred or mixing vessels to use the mixing Reynolds number, Re_m to characterise the flow

$$Re_m = \frac{\rho D^2 N'}{\mu} \quad (13)$$

where D is the diameter of the impeller and N' is the number of revolutions per second. For $Re_m > 10,000$, the flow is assumed to be fully turbulent. In the present application, with the least viscous fluid and the highest impeller speed, the mixing Reynolds number is approximately 100, which indicates all simulations are laminar.

For the spindle geometry, smooth, no slip wall boundary conditions were applied to the inner, outer and bottom walls. The upper boundary was set as a symmetry plane as the shear between air and bitumen is insignificant. A moving mesh approach was used, where the entire fluid domain was rotated about the vertical z axis at the appropriate angular velocity, while the outer wall was held stationary relative to the moving zone. The reason for doing this, rather than simply moving the outer wall relative to a stationary fluid domain was so that animations for the DHI impeller could be produced with the helices being seen in motion. There was no significant computational overhead associated with the approach used.

The geometry of the spindle was developed based on the Brookfield SC4-27 and realised with ANSYS DesignModeler. A mesh consisting of tetrahedra and triangular prisms (in the inflation layers adjacent to walls) was generated using ANSYS Meshing and the volume mesh associated with the surface mesh shown in Fig. 5 contains 155,000 cells.

The DHI geometry was designed to create a convective like flow within the sample, which allows the uniform distribution of suspended solids within a viscous fluid. The idea is that the outer helix pumps the fluid downwards while the inner helix pumps it upwards. Based on the prototype design, DesignModeler and Meshing were used to produce a mesh, which, due to the increased complexity of the design, contained approximately 1300,000 tetrahedral and triangular prism cells. The CAD model and associated surface mesh can be seen in Fig. 6. A mesh convergence study was conducted with the DHI geometry and key flow parameters at monitoring points were found not to change as the number of cells increased above the 1.3 million of the mesh shown in Fig. 6.

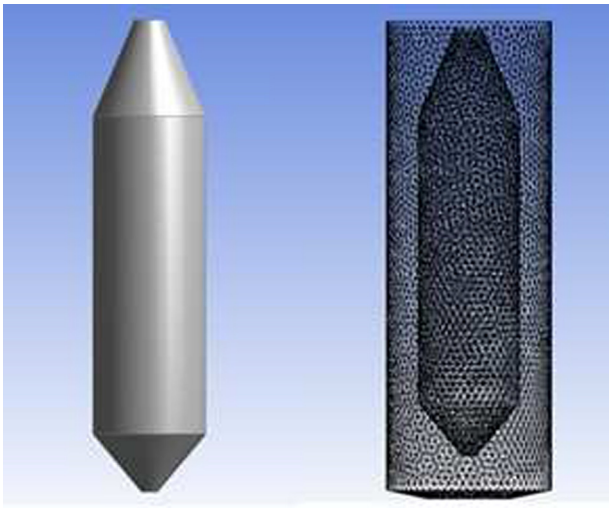

Fig. 5. On the left, a solid model of the Brookfield SC4-27 spindle; and on the right, the surface mesh on the spindle and outer wall.

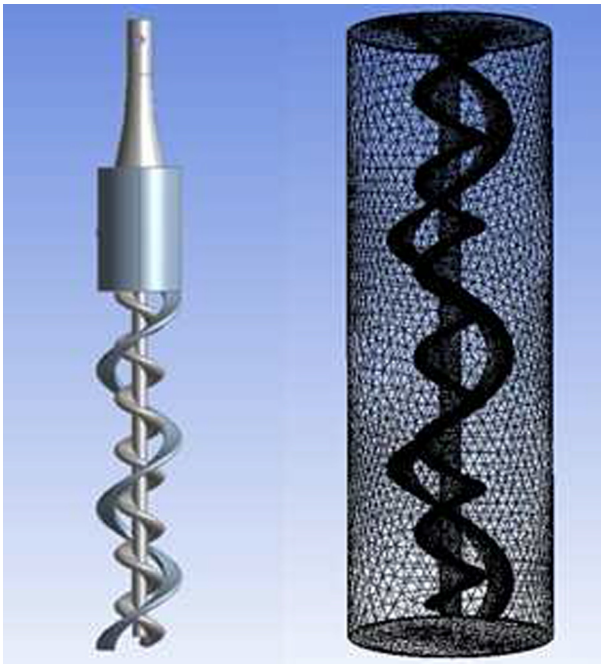

Fig. 6. On the left, a solid model of the DHI mixer; and on the right, the surface mesh on the mixer and outer wall.

Standard solver settings were used throughout: the SIMPLE algorithm was used for pressure–velocity coupling; the Least Squares Cell Based discretization for gradients and second order differencing for the momentum and volume fraction equations. Due to the use of a moving mesh, the solution was necessarily transient and it was found that the simulations had to be run for ~60 s of real time to achieve a stationary solution, where the mean velocity and volume fraction did not drift with time, as measured at a number of monitoring points. The exact run time varied depending on fluid properties and rotation rate.

3. Results

3.1. Experimental

In the manufacturing of rubberized bitumen, the process can take up to 2 h, at which point the particles have swollen to their maximum extent. However, in these experiments, in certain cases (i.e. for the f10 fluid with 400 μm particles) the particles were already settling after a few seconds. It was decided that a testing period of 10 minutes was sufficient to resolve the settling process without the swelling of the particles compromising the results.

Figs. 7 and 8 show images of the distribution of the particles within the blend at the start of the tests and after 10 minutes of rotation for the f100 and f500 fluids respectively. These figures show that using the lower viscosity fluid, f100, at 10 rpm both standard spindle and the DHI do not maintain particles in suspension. At 100 and 200 rpm it is interesting to note how, due its shape, the standard impeller creates two layers of crumb rubber particles on top and bottom. In this case, the particles are forced to migrate from the narrow gap into regions where the swirl is less intense.

However, at these higher rotation rates, the DHI creates a more even distribution of particles. Observations confirmed that this was

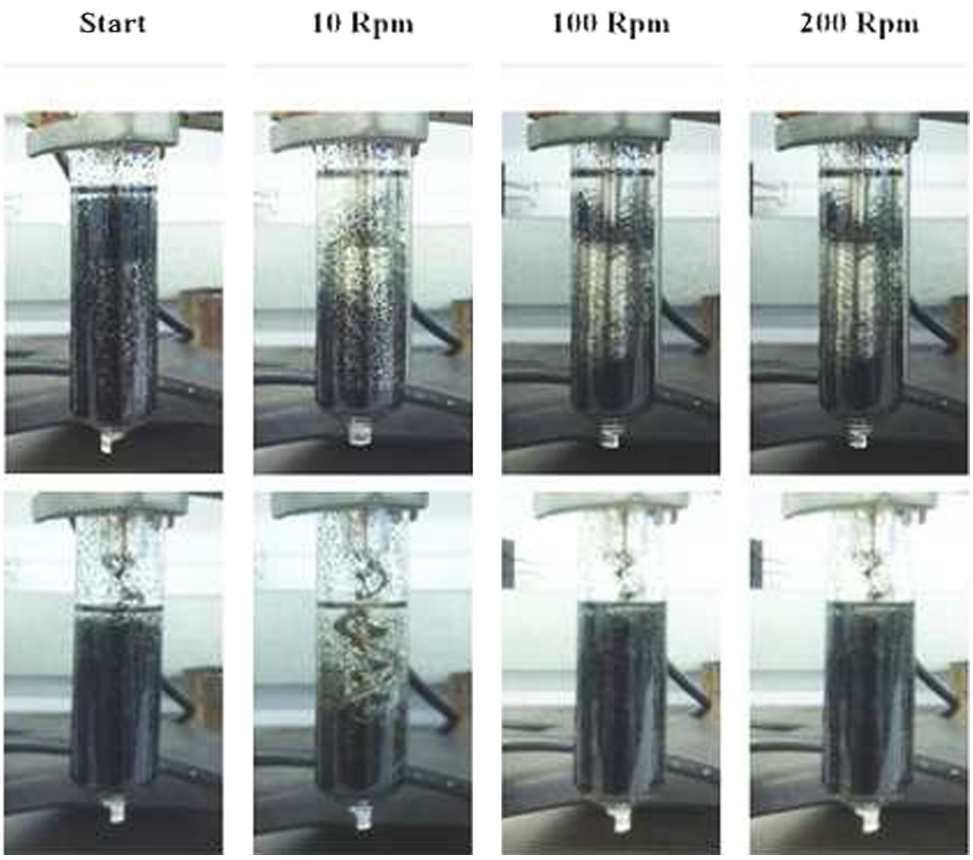

Fig. 7. Images of the distribution of particles in the viscometer using the f100 fluid for the SC4-27 spindle (top) and DHI (bottom) at the start of the test and after 10 minutes for various rotational speeds.

a result of a combination of effects consisting in the inner spiral transporting the particles upwards while the outer thread moves the particles back down – confirming that the design was working as intended. As a result, particles are circulated throughout the container and phase separation is avoided for the whole duration of the experiment.

These results show that the rotational speed is of fundamental importance when considering the extent to which the sample is homogenised and plays a crucial role in determining the efficacy of the impeller. This, of course, has significant consequences on the viscosity readings, which are a function of testing geometry, rotational speed and applied torque.

Fig. 9 shows that the apparent viscosity measurements are independent of the rotational speed for the DHI than the SC4-27 spindle (apart from at 10 rpm). The fact that the curves for 100 and 200 rpm are convergent for the DHI echoes the observations made about Fig. 7, where the higher rotational speeds produce a less heterogeneous blend. At 10 rpm, there is clearly some intermittency to the viscosity measurements as the particles do not reach a steady-state distribution. In any case, both viscosity values over time and shear dependency, play in favour of the DHI, which seems to provide more stable rheological information of this complex system – itself an indication of the better mixing efficiency over the timescale of the test.

For the higher viscosity fluid, f500, over the same timescale, these observations are not so clear (Fig. 10). In this test, all viscosity measurements are still increasing after 600 s, suggesting that the particles were still undergoing redistribution or possibly the swelling process is starting, especially at the higher rotational speed. Indeed, the absence of a 200 rpm result prevents the same conclusion being drawn for convergence of the viscosity results as the rotation speed is increased above 100 rpm. Indeed, after 20 minutes (1200 s) the viscosity had still not settled down to a consistent value. Unfortunately, running the tests for a longer period meant that the temperature of the mixture would begin to drop and viscosity measurements would then have a temperature component. Again, however, the viscosity trend with time still favours the DHI.

3.2. CFD simulations

3.2.1. Validation (Single Phase)

While not presented here, it should be noted that the CFD model of the SC4-27 spindle produced values of SRC and SMC that were very close (within 1%) as those quoted in the Brookfield literature for a range of rotational speeds and fluid viscosities.

Then, for the DHI geomerty, in an attempt to reproduce the single phase experimental testing of Lo Presti et al. [19], a number of single phase simulations were performed. The rotational speed of the impeller was again varied as too was the viscosity of the fluid. Values of both the rotational speed and dynamic viscosity were matched to those used by Lo Presti et al. [19] as closely as possible. The dynamic viscosity values used were 0.0094, 0.098, 0.488, 0.970 and 5.040 Pa s, while rotational speeds of 10, 50, 100 and 200 rpm were chosen. Thus, in total, 20 simulations were performed. In order to be able to compare across this range of viscosity and rotational speed, the mixing Reynolds number, Eq. (13), was used with an equivalent diameter of 11.7 mm. The choice of the diameter is somewhat arbitrary and corresponds in this case to the diameter of the SC4-27 spindle, although it is a value roughly halfway between the inner and outer helices of the DHI. The SMC values are calculated from a re-arrangement of Eq. (5), via a conversion

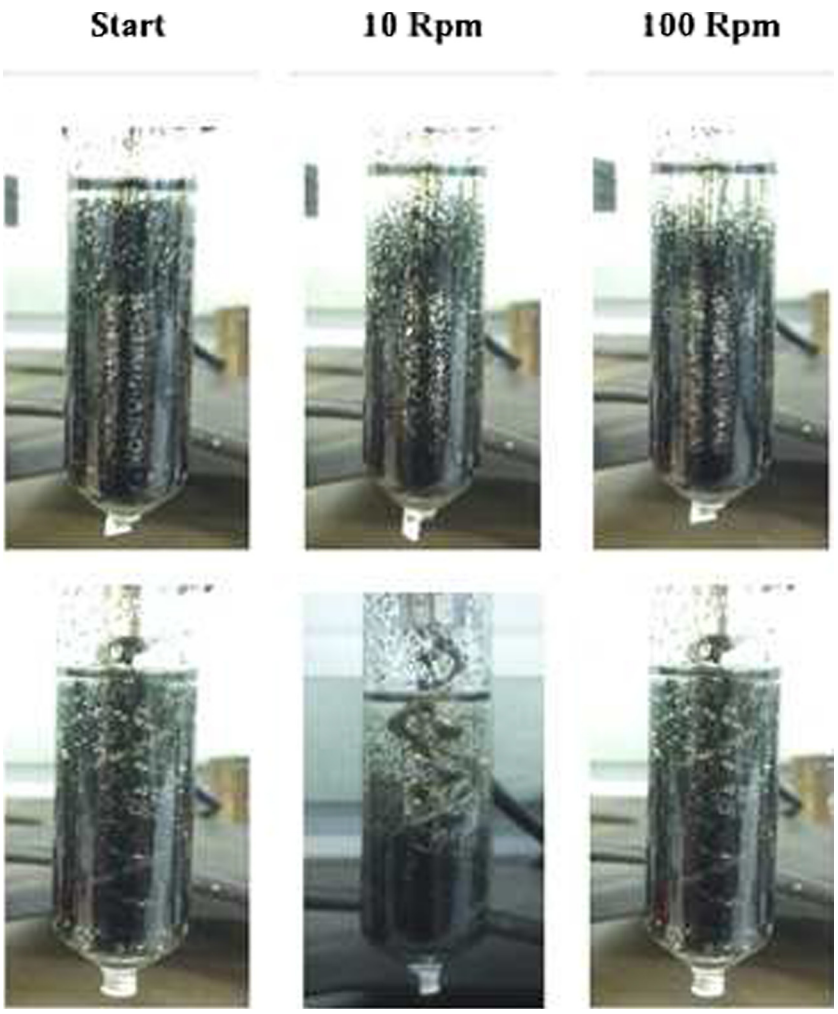

Fig. 8. Images of the distribution of particles in the viscometer using the f500 fluid for the SC4-27 spindle (top) and DHI (bottom) at the start of the test and after 10 minutes for various rotational speeds.

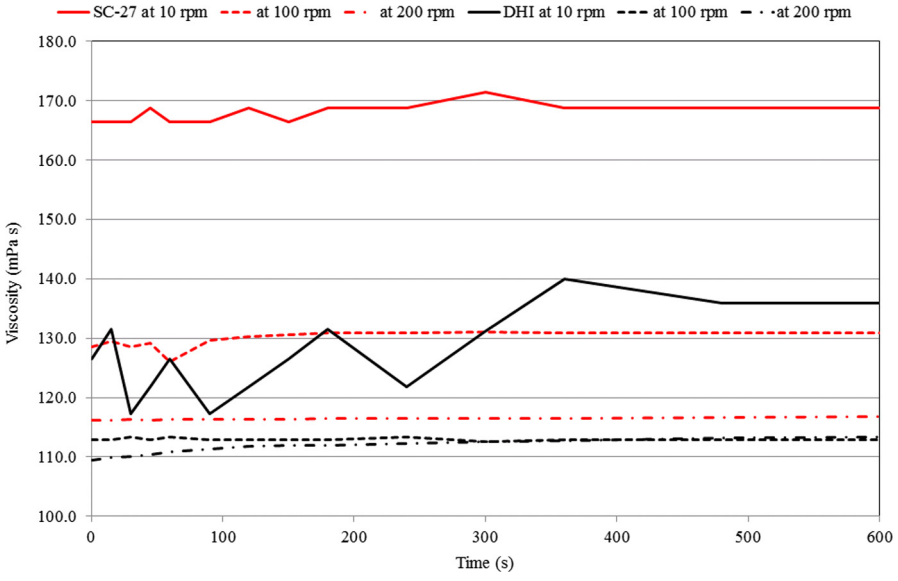

Fig. 9. The variation of viscosity with time during the tests for the SC4-27 spindle and DHI at 10, 100 and 200 rpm using the f100 fluid.

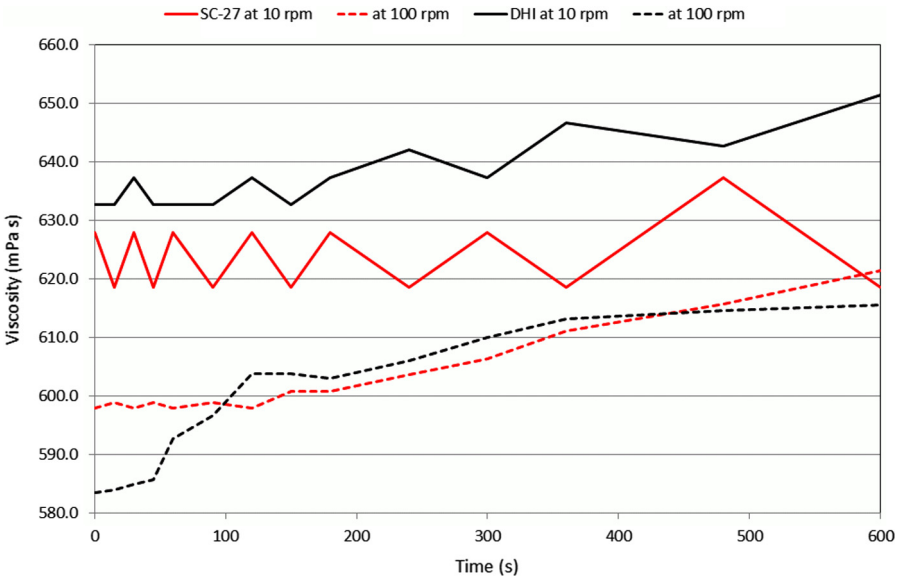

Fig. 10. The variation of viscosity with time during the tests for the SC4-27 spindle and DHI at 10 and 100 rpm using the f500 fluid.

of the torque that Fluent reported to an equivalent percentage torque, T%, reported by the Brookfield viscometer.

Fig. 11 shows a clustering of the SMC values around a value of 50, across a 5 decade range of Reynolds numbers. Note that the value of SMC that Lo Presti et al. [19] found for the DHI was 50 and so there is quantitative agreement between the experiment and simulations. What the numerical modelling reveals, however, is that at a fixed rotational speed, there is a dependency on the Reynolds number, the extent of which is reduced at the highest rotational speed of 200 rpm. Similarly, we see that for a fixed value of viscosity there is a marked increase in SMC as the rotational speed is increased. This can be seen in the clustering of results in lines comprised of the four symbols from left to right. There are several explanations for this functional dependence of SMC on Re_m. First since the same mesh was used for all simulations, the local cell Reynolds numbers would differ from simulation to simulation, which may result in a numerical errors being introduced.

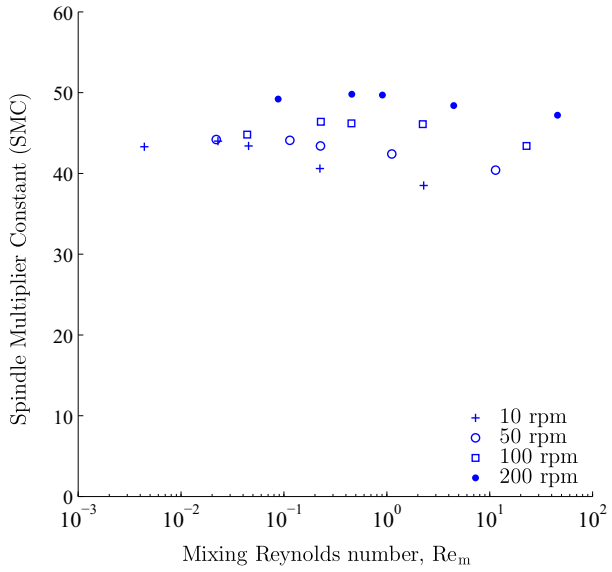

Fig. 11. Plot of the Spindle Multiplier Constant (SMC) against mixing Reynolds number for the DHI impellor.

Second, from the physical perspective, it is thought that the variations are down to the flow patterns changing across the range of Reynolds numbers. There is some experimental evidence to back this up. With reference back to Fig. 7, it can be seen that the DHI produces more consistent mixing at a rotational speed of greater than 100 rpm. This may be attributed to the impeller producing a different flow field, a more efficient flow field from the mixing perspective, that at 10 rpm. This difference may explain the function dependence of SMC on the mixing Reynolds number.

3.2.2. Understanding the DHI mixing process (multiphase)

When considering all the combinations of parameters in the experimental tests discussed in Section 3.1, it became apparent that there were two distinct sets of cases: those with stratification of the particulate phase and those where homogeneous mixing was observed. Thus, the numerical modelling focused on the cases where these extremes were exhibited. Table 2 shows the range of simulations that were run with a ♢ indicating those cases where phase stratification was expected and a • where a level of homogeneity in the secondary phase distribution was expected. The two gaps in the table are due to the high viscosity of the f500 preventing the viscometer from operating under those conditions. In all cases the volume fraction of the particulate phase was 3 % and the diameter of the particles was 400 μm.

Before considering the mixing efficiencies of the two designs, it is instructive to look at the velocity fields in both cases. Fig. 12(a) shows contours of the steady-state velocity magnitude for the SC4-27 spindle. The SC4-27 creates a Taylor–Couette flow between the rotating spindle and the stationary wall. There is a large circumferential or swirling component to the flow but not a vertical component. As such, particulates in the flow are not driven vertically through the gap (in either direction) but rather tend to sink to the bottom under the effects of gravity.

On the other hand, the instantaneous velocity field for the DHI, Fig. 12(b), presents a far more complex picture. Here the plot is showing a snapshot of the velocity magnitude and what cannot be gleaned from this plot that the outer helix is moving fluid downwards, while the inner one is moving fluid upwards. This becomes clear in Fig. 13, in which the vector length is constant but the colour represents the local velocity magnitude (blue is zero, red is 0.061 m s^{-1}). While the figure shows only the vectors on a vertical

Table 2
The CFD simulations (♢ indicates cases where experimentally there was phase stratification, • where there was a good level of mixing).

	SC4-27			DHI		
Fluid	10 rpm	100 rpm	200 rpm	10 rpm	100 rpm	200 rpm
f100	♢	♢	♢	♢	•	•
f500	♢	•		♢	•	

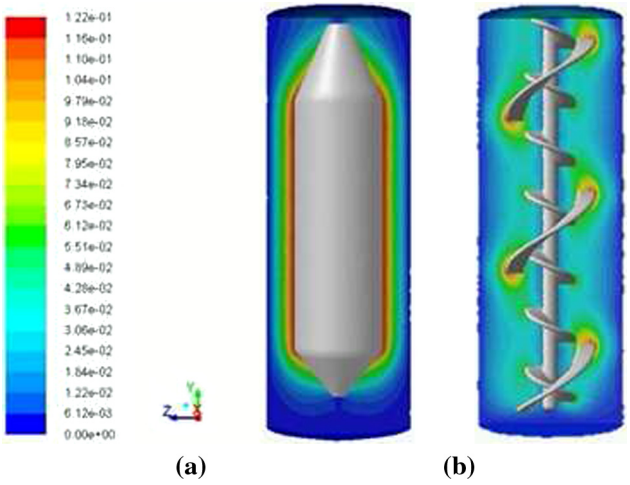

Fig. 12. Contours of velocity magnitude for the (a) SC4-27 spindle and (b) DHI (right) at 100 rpm.

plane and the view focusses on the mid-height region, the flow is now entirely 3D in nature and the simple observations and theory associated with Taylor-Couette flow are no longer possible.

To gain a better understanding of the degree of homogenisation, the volume fraction of the particulate phase was evaluated once the volume fraction for both types of spindle had reached a steady-state. For the DHI, while the velocity is not steady, the distribution of particles does reach something very close to a steady state because of the very low settling velocity of the particles in the highly viscous fluids under consideration. Qualitatively, the

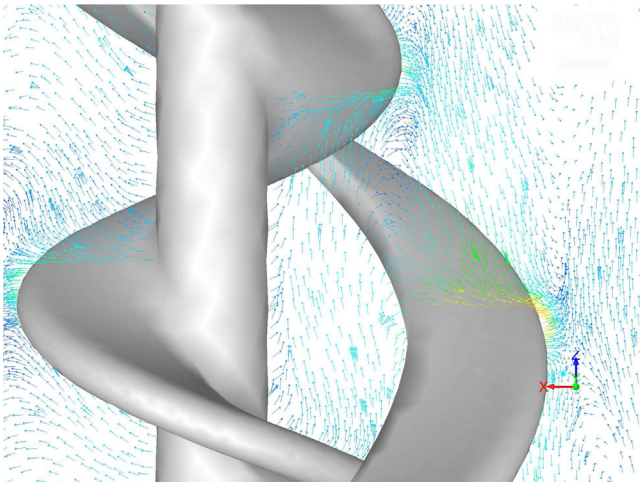

Fig. 13. A close-up of the inner and outer helices of the DHI impellor, showing the flow vectors on the plane $y = 0$. Vectors are the same length and the velocity magnitude is indicated by the color (blue is zero, red is 0.061 m s^{-1}). (For interpretation of the references to colour in this figure legend, the reader is referred to the web version of this article.)

results from the numerical simulations, compared very favourably with the experimental results.

Fig. 14 shows the results achieved using the f100 and f500 fluids at different rotational speeds for both the CFD model and the experimental tests. With reference to the figure, the contour plots of the volume fraction of the particulate phase do bear some similarity to the photographs from the experiments that are shown below them. The highly concentrated zone of particles near the bottom of the container (indicated by the red region, which corresponds to a volume fraction of 0.08) becomes less apparent when the angular velocity of the spindle and the viscosity of the fluids are increased. In fact, the contour range is clipped to a maximum of 0.08, so although the zone for the f100, 10 rpm case looks small, it is in fact a very small region of very high concentrations. In this case, the suspended particles are able to sink to the bottom and concentrate on the central region where fluid motion is minimal – see Fig. 12(a).

There is still some stratification of the secondary phase in all the plots in Fig. 14, which is also apparent in the experimental results. Two effects are not captured by the CFD model, however. First, the floating scum of particles on the surface of the liquid are not seen because the top boundary of the CFD domain is a symmetry boundary – these particles are held there by surface tension effects, which are not included in the numerical model. Second, the CFD model does not show the that some particles stay above the narrow Couette flow region, as well as falling below it. The gap between the spindle and the container wall seems to prevent the particles from settling out, at least on the time scales over which the experiments were run.

The CFD model confirms that the main issue of using the standard spindle is that it causes phase separation between the particles and bitumen leading to misleading viscosity measurements. This is due to the absence of vertical components of velocity in what is essentially a flow regime with cylindrical symmetry. Increasing the fluid viscosity (f500) can also lead to a more homogeneous distribution of particles in the liquid and reduces the phenomenon of particles concentration on the bottom. However, it is not clear that this enhanced mixing is not simply due to the lower terminal velocity of the particles in the more viscous fluid. A look at Fig. 10 would indicate that the apparent viscosity for the f500, 100 rpm case had not settled to a constant value and thus a longer test may have produced more stratification.

A very different picture generally emerges when considering the DHI impeller (Fig. 15). There is qualitative agreement between the CFD and experimental data in this case. However, at 10 rpm, the DHI still produces a noticeably stratified particulate phase. Again, due to the clipping of the volume fraction at 0.08, the fact that the red region (indicating volume fractions above 0.08) is larger than for the SC4-27 cases, then there is some agitation of the fluid in this region. This agitation is sufficient to keep the particles partially suspended above the base of the viscometer. Nonetheless, this level of mixing is not sufficient to render any apparent viscosity measurements reliable. At 100 rpm, a level of homogeneity is seen in the particulate phase, which indicates that the impeller is performing its intended task, which is to mix the particulate phase throughout the device.

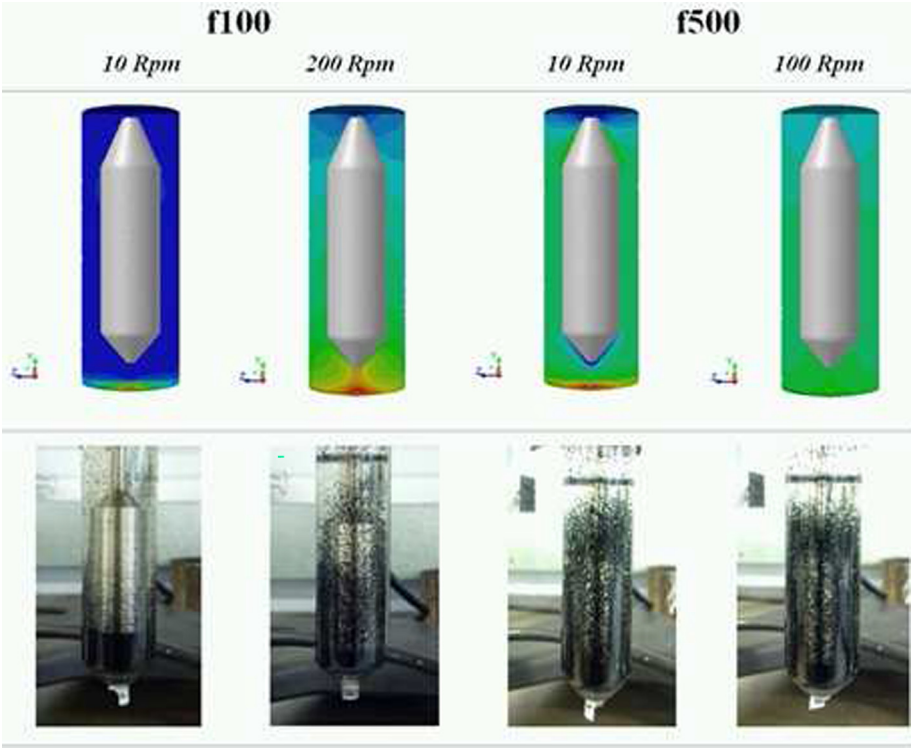

Fig. 14. Volume fractions from the CFD model (top) and experimental images (bottom) for the SC4-27 spindle. The volume fractions range from 0 (blue) to 0.08 (red). (For interpretation of the references to colour in this figure legend, the reader is referred to the web version of this article.)

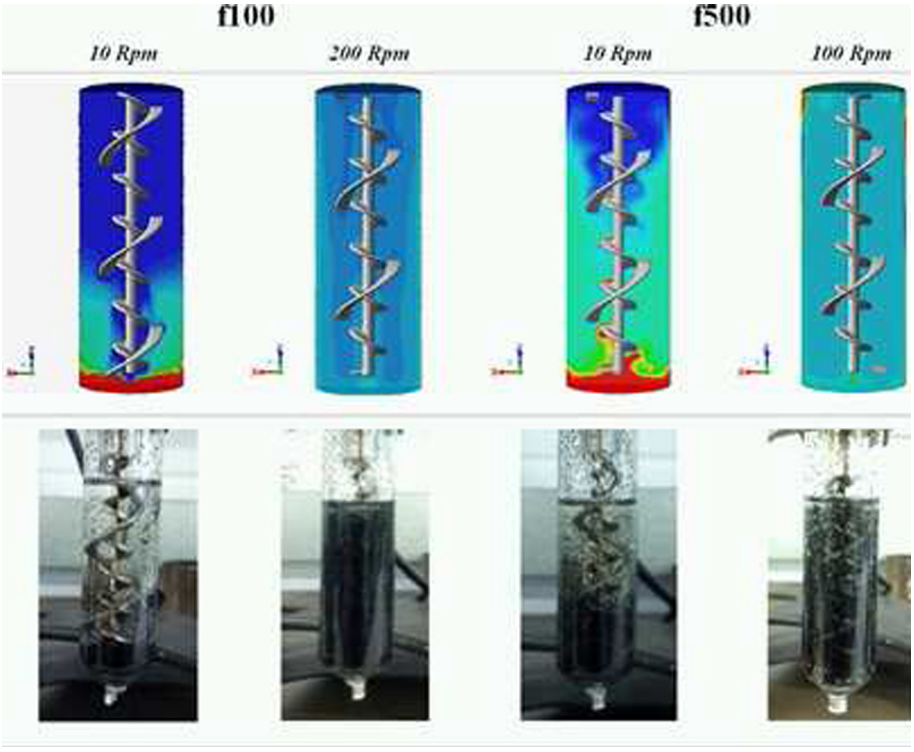

Fig. 15. Volume fractions from the CFD model (top) and experimental images (bottom) for the DHI. The volume fractions range from 0 (blue) to 0.08 (red). (For interpretation of the references to colour in this figure legend, the reader is referred to the web version of this article.)

4. Conclusions

In this study, the authors used customised laboratory testing and computer simulations to gain a deeper understanding of the fundamental mechanisms behind the improved viscosity measurements obtained when using the DHI with rubberised bitumen. Furthermore, this study look closely at the phase separation issues that can occur in a wide range of complex fluids. Overall, the following conclusions can be drawn:

- The experimental programme provided a clearer picture of the mixing enhancement provided by the DHI when measuring multiphase fluids composed of a liquid and a suspended particulate phase. Furthermore, the DHI geometry allows obtaining a steady apparent viscosity measurement and requires lower torques. This extends the range of measurable viscosity when compared to the standard spindle, SC4-27.
- CFD simulations clarified the mechanisms behind the previously assumed convective flow created by the DHI. In fact, the analysis of the velocity fields confirms that the central screw of the DHI drags up the complex system while the external screw transports the mixture downwards. Results also highlighted that with current design, the central screw of the DHI could be more effective at pumping the fluid vertically – this leads the way to enhancements in the design.
- The single phase CFD simulations produced values of SMC that were in close agreement with the experiments of Lo Presti et al. [19]. In summary, CFD helped to gain insights in the complex flow regimes and shows potential to be used as a platform to design new testing geometries for complex fluids as well as for virtual rheology measurements. In the next future, researchers should look with confidence in using CFD as platform for improving rheometry of complex fluids. The DHI showed to be a significant step forward from the testing geometries currently used for viscosity measurements of complex fluids, especially within product development. The author are looking at improving the current design as well as performing a campaign aimed at experimentally testing the viscometer for a variety of standard viscosity fluids with different particle loadings and diameters, as well as using complex systems with different rheological properties. This will allow to produce a library of results that will mean this rheometry can be used effectively in the bitumen and other industries for product development and quality control of these type of complex systems.

Acknowledgement

The authors wish to thank the University of Nottingham for the generous funding provided to support this research at two stages through the Bridging the Gaps feasibility award 2012 and the HERMES fellowship 2014. Furthermore, a special thanks goes to Mr. Clive Dixon who allowed customisation of the glass small sample containers. This work was supported by the Engineering and Physical Sciences Research Council (EPSRC) [grant number EP/M506588/1].

References

[1] ASTM. Standard test method for viscosity determination of asphalt at elevated temperatures using a rotational viscometer. American Society for Testing and Materials, a. D4402/D4402M.
[2] ASTM. Standard test method for measurement of apparent viscosity of asphalt-rubber or other asphalt binders by using a rotational hand held viscometer. American Society for Testing and Materials, b. D7741/D7741M.
[3] F. Barailler, M. Heniche, P.A. Tanguy, CFD analysis of a rotor-stator mixer with viscous fluids, Chem. Eng. Sci. 61 (9) (2006) 2888–2894, http://dx.doi.org/10.1016/j.ces.2005.10.064.
[4] F. Bertrand, P.A. Tanguy, E. Brito De La Fuente, P. Carreau, Numerical modeling of the mixing flow of second-order fluids with helical ribbon impellers, Comput. Methods Appl. Mech. Eng. 180 (3) (1999) 267–280, http://dx.doi.org/10.1016/S0045-7825(99)00169-3.
[5] Brookfield. More Solutions to Sticky Problems. Brookfield Engineering Labs., 2014.
[6] CALTRANS. Quality Control Manual for Hot Mix Asphalt. Department of Transportation, State of California, 2011.
[7] B. Celauro, C. Celauro, D. Lo Presti, A. Bevilacqua, Definition of a laboratory optimization protocol for road bitumen improved with recycled tire rubber, Constr. Build. Mater. 37 (2012) 562–572, http://dx.doi.org/10.1016/j.conbuildmat.2012.07.034.
[8] P.J. Cullen, C.P. O'Donnell, M. Houška, Rotational rheometry using complex geometries – a review, J. Texture Stud. 34 (1) (2003) 1–20, http://dx.doi.org/10.1111/j.1745-4603.2003.tb01052.x.
[9] G. Delaplace, J.C. Leuliet, V. Relandeau, Circulation and mixing times for helical ribbon impellers. Review and experiments, Exp. in Fluids 28 (2) (2000) 170–182, http://dx.doi.org/10.1007/s003480050022.
[10] G. Delaplace, R. Guerin, J.-C. Leuliet, R.P. Chhabra, An analytical model for the prediction of power consumption for shear-thinning fluids with helical ribbon and helical screw ribbon impellers, Chemical Engineering Science 61 (10) (2006) 3250–3259, http://dx.doi.org/10.1016/j.ces.2005.11.069.
[11] C. Devals, M. Heniche, K. Takenaka, P.A. Tanguy, CFD analysis of several design parameters affecting the performance of the Maxblend impeller, Computers & Chemical Engineering 32 (8) (2008) 1831–1841.
[12] R.B. Dow, The rheology of lubricants, Journal of Colloid Science 2 (1) (1947) 81–91.
[13] C. Gallegos, J.M. Franco, Rheology of food, cosmetics and pharmaceuticals, Current Opinion in Colloid & Interface Science 4 (4) (1999) 288–293, http://dx.doi.org/10.1016/S1359-0294(99)00003-5.
[14] G. Havas, J. Sawinsky, A. Deak, Investigation of the homogenization efficiency of the screw agitator, helical ribbon agitator, gate type anchor impeller and the multi-paddle agitator in the mixing of high-viscosity Newtonian liquids, Chemical Engineering 22 (4) (1978) 317–330.
[15] A. Iranshahi, M. Heniche, F. Bertrand, P.A. Tanguy, Numerical investigation of the mixing efficiency of the Ekato Paravisc impeller, Chem. Eng. Sci. 61 (8) (2006) 2609–2617, http://dx.doi.org/10.1016/j.ces.2005.11.032.
[16] A. Iranshahi, C. Devals, M. Heniche, L. Fradette, P.A. Tanguy, K. Takenaka, Hydrodynamics characterization of the Maxblend impeller, Chem. Eng. Sci. 62 (14) (2007) 3641–3653, http://dx.doi.org/10.1016/j.ces.2007.03.031.
[17] Shew-Fen Lin, Robert S. Brodkey, Rheological properties of slurry fuels (1978-present), J. Rheol. 29 (2) (1985) 147–175.
[18] D. Lo Presti, G. Airey, Tyre rubber-modified bitumens development: the effect of varying processing conditions, Road Mater. Pavement Des. 14 (4) (2013) 888–900, http://dx.doi.org/10.1080/14680629.2013.837837.
[19] D. Lo Presti, C. Fecarotti, A.T. Clare, G. Airey, Toward more realistic viscosity measurements of tyre rubber–bitumen blends, Constr. Build. Mater. 67 (2014) 270–278, http://dx.doi.org/10.1016/j.conbuildmat.2014.03.038.
[20] A.Y. Malkin, The state of the art in the rheology of polymers: achievements and challenges, Polym. Sci. Ser. A 51 (1) (2009) 80–102, http://dx.doi.org/10.1134/S0965545X09010076.
[21] Mikko Manninen, Veikko Taivassalo, Sirpa Kallio, et al. On the mixture model for multiphase flow, http://www.vtt.fi/inf/pdf/publications/1996/P288.pdf, 1996, VTT publications 288.
[22] W.I. Patterson, P.J. Carreau, C.Y. Yap, Mixing with helical ribbon agitators: Part II. Newtonian fluids, AIChE J. 25 (3) (1979) 508–516, http://dx.doi.org/10.1002/aic.690250317.
[23] E.L. Paul, V. Atiemo-Obeng, S.M. Kresta, Handbook of Industrial Mixing: Science and Practice, John Wiley & Sons, 2004.
[24] M. Robinson, P.W. Cleary, Flow and mixing performance in helical ribbon mixers, Chem. Eng. Sci. 84 (2012) 382–398, http://dx.doi.org/10.1016/j.ces.2012.08.044.
[25] M. Sommerfeld, S. Decker, State of the art and future trends in CFD simulation of stirred vessel hydrodynamics, Chem. Eng. Technol. 27 (3) (2004) 215–224, http://dx.doi.org/10.1002/ceat.200402007.
[26] A. Subhy, D. Lo Presti, G. Airey, Rubberised bitumen manufacturing assisted by rheological measurements, Road Mater. Pavement Des. 17 (2) (2015) 1–21, http://dx.doi.org/10.1080/14680629.2015.1079549.
[27] G. Tabilo-Munizaga, G.V. Barbosa-Cánovas, Rheology for the food industry, J. Food Eng. 67 (1) (2005) 147–156, http://dx.doi.org/10.1016/j.jfoodeng.2004.05.062.
[28] K. Takahashi, T. Yokota, H. Konno, Mixing of pseudoplastic liquid in a vessel equipped with a variety of helical ribbon impellers, J. Chem. Eng. Jpn. 21 (1) (1988) 63–68, http://dx.doi.org/10.1252/jcej.21.63.
[29] P.A. Tanguy, R. Lacroix, F. Bertrand, L. Choplin, E.B. De La Fuente, Finite element analysis of viscous mixing with a helical ribbon-screw impeller, AIChE Journal 38 (6) (1992) 939–944, http://dx.doi.org/10.1002/aic.690380614.
[30] Y.-Y. Tsui, Y.-C. Hu, Flow characteristics in mixers agitated by helical ribbon blade impeller, Eng. Appl. Comput. Fluid Mech. 5 (3) (2011) 416–429, http://dx.doi.org/10.1080/19942060.2011.11015383.
[31] B.-H. Um, T.R. Hanley, A CFD model for predicting the flow patterns of viscous fluids in a bioreactor under various operating conditions, Korean J. Chem. Eng. 25 (5) (2008) 1094–1102, http://dx.doi.org/10.1007/s11814-008-0179-y.
[32] W. Yao, M. Mishima, K. Takahashi, Numerical investigation on dispersive mixing characteristics of Maxblend and double helical ribbons, Chem. Eng. J. 84 (3) (2001) 565–571, http://dx.doi.org/10.1016/S1385-8947(01)00135-8.
[33] C.Y. Yap, W.I. Patterson, P.J. Carreau, Mixing with helical ribbon agitators: Part III. Non-Newtonian fluids, AIChE J. 25 (3) (1979) 516–521, http://dx.doi.org/10.1002/aic.690250318.